INSTITUTE OF PHYSICS PUBLISHING MEASUREMENT SCIENCE AND TECHNOLOGY

Meas. Sci. Technol. **17** (2006) 1723–1732 doi:10.1088/0957-0233/17/7/010

Integrating nephelometer with a low truncation angle and an extended calibration scheme

A Abu-Rahmah, W P Arnott and H Moosmüller

Desert Research Institute, University of Nevada System, 2215 Raggio Parkway, Reno, NV 89512, USA

Received 12 January 2006, in final form 8 April 2006
Published 7 June 2006
Online at stacks.iop.org/MST/17/1723

Abstract

A resurgence of interest has arisen lately in the use of reciprocal nephelometers in aerosol instrumentation that also measures other optical properties such as extinction by the cavity ringdown method and absorption by the photoacoustic method. This paper provides fresh insight into these nephelometers from perspectives of instrument component evaluation, intra-instrument comparison and basic calibration. In particular, a 4° truncation angle reciprocal integrating nephelometer (IN) is described and demonstrated. An experimental setup for the measurement of the IN sensor cosine response is developed and described. To calibrate the IN, the sampling volume can be filled with an aerosol with negligible light absorption (e.g., ammonium sulfate), and scattering and extinction coefficients are monitored simultaneously. The performance of the IN is evaluated, at a wavelength of 532 nm, through extensive comparison with a 1° truncation angle integrating sphere integrating nephelometer (ISIN) that operates at the same wavelength. The intercomparison included measurements of ambient aerosol, kerosene soot, ammonium sulfate aerosol, NaCl aerosol and CO_2 gas. Results of a linear regression analysis indicate an agreement between the IN and the ISIN within ±8%. The main advantages of the IN over the ISIN are its fast time response, relatively large signal-to-noise (S/N) ratio and design simplicity.

Keywords: integrating nephelometer, modified sensor cosine response, aerosols, light scattering, light extinction

1. Introduction

Aerosol particles in the atmosphere have several important environmental effects. At high concentrations, they represent a health hazard and limit visibility by attenuating visible radiation [1, 2]. They affect the climate of the earth, directly by scattering and absorbing radiation, semi-directly by absorbing radiation and reducing cloudiness and indirectly by serving as nuclei for cloud formation [3].

Interaction of aerosol particles with light forms the basis for a widely used class of instruments, namely nephelometers. The scattered light is usually characterized by nephelometers that utilize an optical scheme for angular integration of scattered light. Beuttell and Brewer [4] devised two techniques to integrate the scattered light intensity geometrically over most of the angular range (i.e., 4π). In the first arrangement a cosine-weighted diffuse light source is used to illuminate the scattering volume that is viewed with a detector. In the second arrangement the detector and light source are reversed, a parallel light beam is used and the scattered light is detected by a cosine detector. The first type is more common while the second arrangement is identified as a reciprocal nephelometer [5–9]. An ideal IN is basically a photometer that measures the total scattering coefficient of atmospheric aerosol over a full angular integration range of 4π. However, existing integrating nephelometers are not ideal and typically integrate over scattering angles ranging from 7° to 170° [5, 8, 10]. These limiting scattering angles are identified as truncation

angles. In particular, light scattered at angles smaller than ∼7° and larger than ∼170° is not detected by most modern integrating nephelometers [10]. The near-forward and near-backward scattered light that is not measured by the detector is a function of the truncation angle (α) and thus is identified as a truncation error. As the angular distribution of light scattered by particles depends strongly on particle size, the total scattering coefficient measured with an IN depends on the instrument's truncation angles.

For particles whose sizes are larger than the wavelength, the scattering phase function is dominated by scattering in the forward direction such that the induced truncation error depends strongly on the particle's size. Several studies, based on Mie scattering calculations, have been made to calculate the truncation errors for different types of scattering particles and for different nephelometer designs [11–16]. In these studies, truncation errors on the order of 10–20% have been found for typical atmospheric aerosol size distributions. It should be emphasized that Mie-based calculations of truncation errors are limited to individual homogeneous spherical particles. Obviously, non-spherical particles are common in the atmosphere and elsewhere. For example, dust particles are generally non-spherical [17] and combustion particles often take the shape of fractal-like agglomerates [18]. Consequently, for non-spherical particles more complex scattering codes are needed to calculate truncation errors as a function of particle shape and size, which is beyond the scope of this paper. Examples of such codes are the discrete-dipole approximation for the calculation of scattering from particles of arbitrary shape [19] and codes based on rigorous solutions extended from Mie theory for agglomerate particles [20, 21].

According to a truncation error analysis done by Moosmüller and Arnott [22], at least half of the light scattered by large particles is due to near-forward diffraction, which may not be detected. Mie calculations have shown that truncation errors resulting from sub-μm particles are small and well correlated with the wavelength dependence of their scattering, while truncation errors for super-μm particles are large and poorly correlated with the wavelength dependence of their scattering [23]. Thus a multi wavelength approach to correct the truncation error for super-μm particles is selective and thus only a partial solution. However, the truncation problem can be solved by reducing the (typical $\alpha = 7°$) truncation angle. Recently a 1° truncation angle integrating sphere integrating nephelometer (ISIN) has been developed. This sevenfold reduction in the truncation angle makes it possible to detect scattering from approximately seven-times-larger particles with an identical truncation error [24]. For light non-absorbing particles with diameters below 16 μm, truncation errors for this nephelometer are less than 25% [22]. The ISIN is a reciprocal nephelometer that uses an integrating sphere with attached truncation reduction tubes to contain the sample volume and to integrate the scattered light.

Though the ISIN is well suited for the measurement of total scattering from ambient coarse particles, its specific design makes it difficult to combine it with an optical technique (e.g. photoacoustic spectroscopy) suitable to measure the absorption component of the extinction coefficient. The purpose of this paper is to describe a relatively simple design with the desired cylindrical geometry that can easily satisfy the stringent requirements of resonance operation of the photoacoustic technique or the interaction length desired for the collinear photothermal technique to monitor the absorption coefficient in the same sampling volume and add it to the scattering coefficient to determine the aerosol extinction coefficient. The instrumental challenge is to achieve a minimum truncation error performance comparable to that of the ISIN and to keep the simplicity of the transmission cell-reciprocal nephelometer (TC-RN) of Mulholland and Bryner [8]. It should be mentioned that the cell geometry of the TC-RN allows collection of scattered light in the angular range 5–175°. It is clear that one should not only optimize the geometry of the sensor to achieve a minimal truncation angle, but also characterize its expected cosine response. In addition, this paper describes a new experimental setup to measure the sensor's cosine response. Recent interest in reciprocal nephelometery coincides with the development of sensitive methods for measuring aerosol extinction by the cavity ringdown technique [25], and aerosol light absorption by the photoacoustic technique [26]. Reciprocal nephelometer sensor heads are placed in these instruments to augment the measurement capability of the single instruments. In the first instrument light absorption is obtained from the subtraction of extinction and scattering coefficients, and in the second, the components of extinction are directly determined by the scattering and absorption measurements. The work described in this paper is relevant to the configurations used in these combined measurement techniques, and as such, it provides a framework for understanding the scattering components of these instruments. This paper is organized as follows. Section 2 provides a description of the reciprocal nephelometer. Section 3 shows the instrument calibration. Section 4 presents kerosene soot measurements. In section 5, we present and discuss an ambient measurement comparison with the ISIN, and in section 6 we conclude the paper.

2. Nephelometer description

The truncation error and non-ideal angular response are the main problems for most of the commercial nephelometers in current use today. Imperfect wavelength response and imperfect aerosol sampling are additional problems. These problems are addressed in the design of the nephelometer described here. Table 1 summarizes the IN design parameters as compared to those of the ISIN. We will refer back to table 1 as the paper proceeds. Figure 1 shows a schematic diagram of the reciprocal integrating nephelometer (IN) developed in this study. The cell, light source and the cosine sensor form the core components of the IN. These components and their selection criteria are described below.

2.1. The cell

To achieve a small instrumental truncation angle, the cell is constructed of a long ($L = 100$ cm) copper tube with an inner diameter D of 2.64 cm. Thus, a sampling volume of about 550 cm^3 is achieved. Relative to the ISIN, which has a sampling volume of about 4200 cm^3, a more than 7.5-fold reduction in volume is accomplished. At a common sampling flow rate for both nephelometers, the IN therefore samples

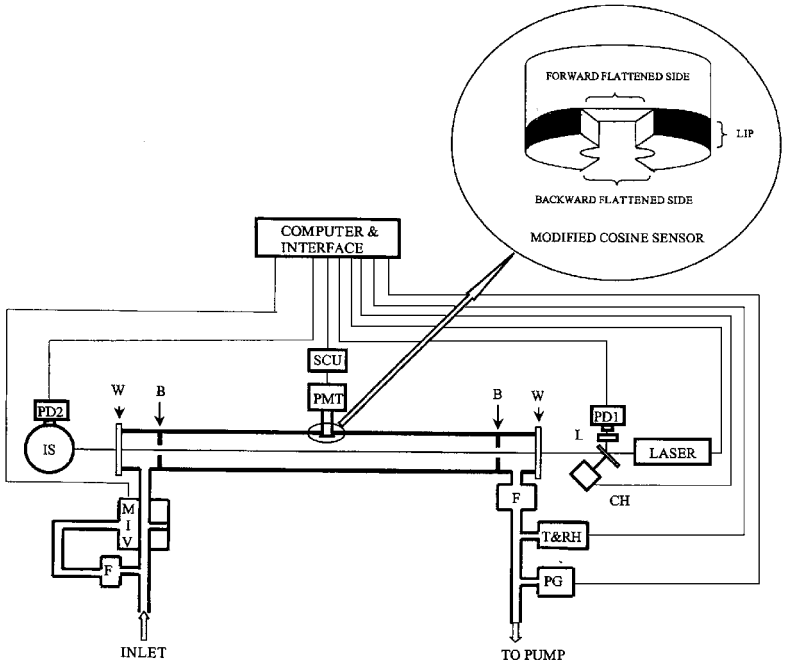

Figure 1. Schematic diagram of the IN. L: lens, CH: chopper, PD_1: photodiode 1, PD_2: photodiode 2, SCU: sensitivity control unit, F: filter, T: temperature, RH: relative humidity, PG: pressure gauge, W: window, B: baffle, MIV: motorized inlet valve, PMT: photo multiplier tube, IS: integrating sphere. In the inset, the modified cosine sensor is shown rotated through 90° about the vertical for detailed illustration.

Table 1. The IN design parameters as compared to those of the ISIN.

Parameter	IN	ISIN
Truncation angle (α)	4°	1°
Sampling volume (V)	~550 cm^3	~4200 cm^3
Flow rate (Q)	3 l min^{-1}	10 l min^{-1}
Measured time response	43 s	105 s
Flow speed at inlet and outlet (υ)	158 cm s^{-1}	212 cm s^{-1}
Reynolds number at inlet and outlet (Re)	662	1400
PMT control voltage (V_{cont})	0.5 V	0.4 V
PMT sensitivity	0.5 V nW^{-1}	0.2 μA nW^{-1}
Wall scattering (W)	50 Mm^{-1}	250 Mm^{-1}
Signal to noise ratio (S/N)	~406	~175

more than 7.5 times faster than the ISIN does. In the middle of the tube, a 0.635 cm diameter hole is drilled to mount the sensor head on the top of the tube. Near each end of the tube, on its side a 0.635 cm diameter hole is drilled for aerosol inlet and outlet. The inlet and outlet are 91.44 cm apart. To reduce wall scattering and for good laser beam and flow confinement, two identical (0.8 cm inner diameter) baffles are mounted inside the tube at 2 cm after the inlet and 2 cm before the outlet respectively. To minimize the reflection of the scattered light and the effect of stray light, the tube's interior is coated with black paint, which allows further reduction of the wall scattering. On both ends of the tube, glass windows are attached to aluminium holders.

2.2. The light source

In most nephelometers, imperfect wavelength response is due to the integration of particle scattering over a wavelength range that is typically 40 nm for commercial nephelometers that use a thermal light source and a bandpass filter [10]. However, employing a laser with a spectral width of a fraction of a nanometre as a light source eliminates the effect of imperfect wavelength response. The comparatively wide bandwidth of commercial nephelometers complicates calibration due to the stronger spectral dependence of light scattering by gases, compared to that of ensembles of particles. Use of thermal light sources also results in substantial heating of the sample volume and concomitant reduction of the relative humidity with possible reduction of the particle size and scattering coefficient.

For the IN developed in this study, a frequency-doubled, continuous-wave, 60 mW, diode-pumped Nd:YAG laser (CrystaLaser model GCL-100-M) operating at a wavelength of 532 nm is used as a light source. In the reciprocal integration method adopted in the design of this nephelometer, the scattering function depends on the direction of polarization of the incident laser beam. To make the measurements independent of polarization, either of two methods can be used: first, a quarter wave plate rotator circularly polarizes the laser beam [7]. Second, a laser light source polarized at 45° relative to the plane defined by the laser beam and the centre of the detector is equivalent to natural (unpolarized) light as the sum of two orthogonal, equal amplitude, linearly polarized waves [8]. The second method is used in this nephelometer to eliminate the effect of polarization on the scattering coefficient.

2.3. The sensor

The light flux detected by an ideal cosine sensor is proportional to the product of the incident light intensity and cos φ (φ is the angle between the scattering direction and the normal to the detector surface). A two-dimensional aperture would have a perfect cosine response,

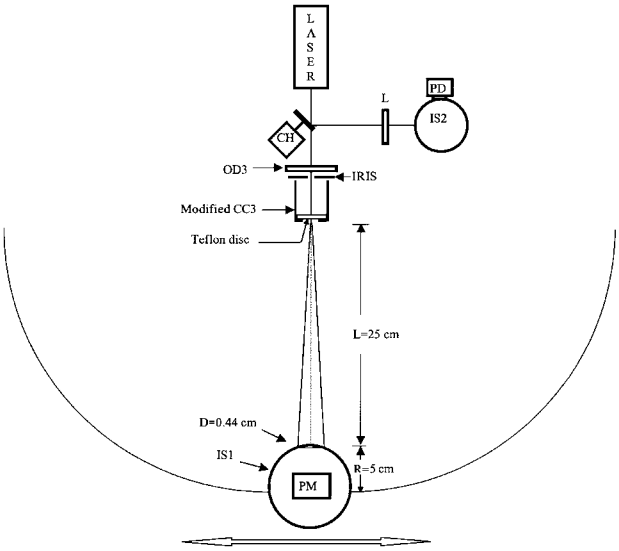

Figure 2. Schematic diagram of the experimental setup used in this study to measure the cosine response of the sensors. OD3: optical neutral density filter.

since the flux entering the aperture is proportional to the projected area, which in turn is proportional to cos φ. Once the two-dimensional aperture is covered with a transparent material, the flux of light penetrating it and passing through the aperture is no longer simply proportional to cos φ. At each angle, some fraction of the light is reflected in addition to being diffracted with an increasing fraction being reflected as the angle φ approaches 90° [8]. In practice, two-dimensional apertures do not exist and an aperture of finite thickness would have large scattering from its edges.

To compensate for such an effect, a sensor consisting of a photomultiplier tube (PMT) and a physical cosine corrector (CC) was employed. In this nephelometer a modified CC3-UV (Ocean Optics Inc.) cosine corrector is attached to a Hamamatsu H5784-01 PMT via an approximately 2 cm long, 0.63 cm diameter blackened tube. The CC3-UV has a teflon disc of 0.03 inch thickness that sits at the end of the tube. Teflon is a strongly scattering material that provides a near-cosine response. Over the wavelength range of 200–1100 nm, it provides optimum light diffusion.

Figure 2 shows the experimental system, used in this study, to measure the cosine corrector response. In this system, the laser beam illuminates the interior side of the teflon disc and a PMT is attached to the top of a 5 cm radius integrating sphere (IS1) that revolves around the sensor in a semicircle of 30 cm radius ($R + L$). While traversing the full angular range of 0–180°, IS1 receives the diffused light intensity from the teflon disc through a 0.44 cm diameter opening carefully aligned at 0° to face the teflon disc. At these configurations the viewing angle of IS1 is approximately 1°. Thus, intensity changes resulting from fine increment (2°) or coarse increment (10°) rotations of the IS around the sensor are both measurable and much larger than changes resulting from electronic noise. A chopper blade set at 45° relative to the incident laser beam is used to both modulate and monitor the power by periodically reflecting it to IS2. To keep the PMT far from saturation, an optical neutral density filter (OD3) is used to reduce the incident laser power. In addition, an iris is used in the beam path between the chopper and the sensor to reduce edge diffractions from the chopper blade. It should be emphasized that the above-described technique to quantify the sensor's response is reciprocal to the original process that takes place in the IN. In other words, in the IN, the PMT is attached to a fixed sensor that receives scattered light intensity across a wide angular range. Due to its ease of alignment, the reciprocal technique is used to measure the cosine response of the sensor. This entails switching light source (laser) and detector. Due to the reversibility of the light propagation (in the absence of strong magnetic fields) this setup yields results identical to the direct measurement.

According to the manufacturer's (Ocean Optics) specification sheet, the original CC3-UV tube is 'lipped' to collect radiation (light) over about 180°, eliminating optical interface problems associated with the light collection sampling geometry. However figure 3(*a*) shows that the response of this sensor, measured using the reciprocal technique described above, suffers a truncation angle of approximately 10° associated with its edges (lip). In addition, this sensor was implemented in the IN to monitor the scattered light intensity from ambient air and several comparisons with the ISIN showed a truncation error of about 30%. To improve its light collecting geometry, the original CC3-UV lip was flattened out in both forward and backward directions as depicted in the inset of figure 1. The cosine response of the modified CC3-UV is measured using the same reciprocal technique. Figure 3(*a*) shows the modified response curve as compared to that of the original CC3-UV and to that of the ideal cosine with all curves normalized to 1 at 0°. Defining the truncation angle as that associated with a cutoff error of 60%, it can be seen that the truncation angle is reduced to about 4°. It should be mentioned that this definition of the truncation angle is associated with the sensor's light-collecting geometry and is based on the new experimental method for characterizing the sensor's cosine response. Figures 3(*b*) and (*c*) show details of the response curve in the critical near-forward/backward scattering regions near ±90°. The cosine response of this sensor is wider than that of the original one. In addition, a series of comparisons between the scattering coefficient measured by the IN, with the modified CC3-UV, and by the ISIN were carried out and showed that the angular truncation error is reduced to be within the range of ±8% for the four types of aerosols listed in table 2.

In many cases, geometrical and technical limitations of the sensor impose restrictions on the length of any nephelometer. In particular, at a specified distance between the sensor and the laser beam, the truncation angle associated with the sensor defines the scattering path length (∼cell length). Increasing the cell's length beyond that defined by the sensor does not provide any further reduction of the overall truncation angle of the instrument. This IN uses the modified CC3-UV sensor to collect radiation from ∼4° to 176°. A matched cell would have a scattering path length of $2h/\tan(4°) = 22$ cm, where $h = 0.76$ cm is the sensor-beam offset of our IN. However, a longer cell, as used in our IN, decreases the wall scattering from the cell windows onto the sensor and allows an improved extinction calibration scheme for light non-absorbing aerosols. Both diffraction and Mie theories are used to estimate the

Table 2. Results of linear regression analysis.

Sample	Sampling time (start–end)	y-axis (Mm^{-1})	x-axis (Mm^{-1})	Slope	Offset (Mm^{-1})	R^2
$(NH_4)_2SO_4$	16:00–17:30	IN-B_{scat}	IN-B_{ext}	1.06	+553	0.99
$(NH_4)_2SO_4$	16:00–17:30	ISIN-B_{scat}	IN-B_{ext}	1.08	+2956	0.98
$(NH_4)_2SO_4$	16:00–17:30	IN-B_{scat}	ISIN-B_{scat}	0.97	−1989	0.99
NaCl	16:40–16:50	IN-B_{scat}	IN-B_{ext}	1.00	+1027	0.97
NaCl	16:40–16:50	ISIN-B_{scat}	IN-B_{ext}	0.99	+1500	0.95
NaCl	15:23–16:50	IN-B_{scat}	ISIN-B_{scat}	0.96	−79	0.99
Kerosene soot	11:00–14:30	IN-B_{scat}	ISIN-B_{scat}	0.97	−4	0.98
Ambient air	48 h	IN-B_{scat}	ISIN-B_{scat}	0.92	−2	0.90

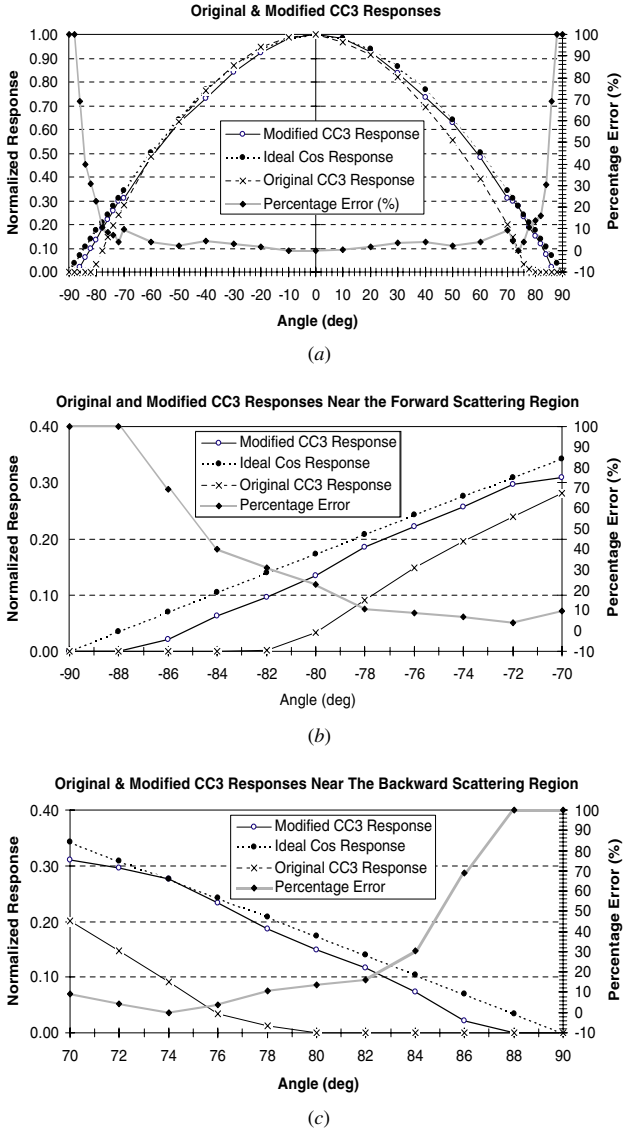

Figure 3. Original and modified CC3-measured angular cosine responses as compared to that of the ideal cosine: (*a*) through the full angular scattering range of 0° to 180°; (*b*) in the critical near-forward scattering region; (*c*) in the critical near-backward scattering region.

forward truncation error as a function of the particle's diameter [24]. At a truncation angle of 4° and for all particles with diameter $D \leqslant 2$ μm, the estimated forward truncation error does not exceed 15% for both absorbing and non-absorbing aerosols with refractive index $m = (1.5, 0.5)$ and $(1.5, 0)$, respectively. The first and second components of the refractive index indicate the particle's real and imaginary components of refractive index.

A small vacuum pump is used to draw the aerosols through the cell of the IN at a constant rate of 3 l min^{-1}. At this flow rate, the Reynold's number ranges from 662 at the inlet and outlet to 159 in the IN interior. Both numbers are much lower than the turbulence threshold. The nephelometer time response is a measure of the time needed to replace the scattering volume inside the cylinder. The estimated time constant is approximately 10 s. Comparing this time constant with that (90 s) of the ISIN developed recently indicates a much faster response for the IN [24]. Due to thermal expansion or contraction in various optical components of the IN, slight misalignments can occur leading to a significant change in the wall scattering. However, this effect is periodically accounted for during sampling time using a motorized inlet valve. This valve is computer controlled at a user-defined interval to automatically alternate between unfiltered and HEPA-filtered air to establish the filtered air background signal. Pressure, temperature and relative humidity are continuously monitored to convert the scattering coefficient to an STP ($P = 1013$ hPa, $T = 273.15$ K) value.

The laser beam is power modulated at a frequency of 500 Hz using a mechanical chopper. The chopper blade is oriented at 45° relative to the laser beam, and its reflectivity has been increased to monitor the incident power with a photodiode (PD_1). The beam is aligned to propagate through the cell's cylinder along its axis. A photodiode (PD_2) attached to a small integrating sphere is used to monitor the transmitted power. A phase-sensitive detector, referenced to the chopping frequency, is used to process the PMT, PD_1 and PD_2 signals. The PMT signal is normalized to the transmitted laser power and converted into a scattering coefficient after instrument calibration.

In the following sections, we validate the measured IN scattering coefficient with that of the ISIN. The ISIN is a novel nephelometer that uses an integrating sphere design with forward and backward truncation angles of 1°. These low truncation angles are achieved through truncation reduction tubes attached on the inlet and outlet of the integrating sphere [24]. The ISIN has been compared with the commercially available Radiance Research M903 and TSI 3563 integrating nephelometers [27, 28], demonstrating good agreement for the measurement of gaseous and fine particle scattering. For coarse particles encountered during a dust entrainment study, the ISIN readings were up to four times higher than those of the RR M903 due to the ISIN's reduced truncation error and coarse particles' sampling losses [27].

3. Calibration

The total scattering coefficient (B_{scat}) is due to Rayleigh scattering by gases (B_{sg}) and scattering by particles (B_{sp}):

$$B_{scat} = B_{sg} + B_{sp}. \tag{1}$$

The nephelometer measures particle light scattering. By measuring the total scattering coefficient and subtracting the gaseous and wall (W) scattering coefficients, the fraction of optical power scattered inside the nephelometer can be calculated as

$$\frac{V_{PMT}}{V_{PD_2}} = C(B_{scat}\ell + W), \tag{2}$$

where C is a proportionality constant, ℓ represents the scattering path, V_{PMT} is the PMT signal voltage and V_{PD2} is the voltage measured across the photodiode that monitors the transmitted laser power. If particle-free air (of scattering coefficient B_{sa}) fills the IN, then

$$\left.\frac{V_{PMT}}{V_{PD_2}}\right|_{\text{filtered air}} = C(B_{sa}\ell + W). \tag{3}$$

Since wall scattering is a common term in both cases it can be eliminated between equations (2) and (3) as

$$B_{sp} = \frac{1}{C}\left(\frac{V_{PMT}}{V_{PD_2}} - \left.\frac{V_{PMT}}{V_{PD_2}}\right|_{\text{filtered air}}\right). \tag{4}$$

In this way, the usual calibration method used, for instance, in the TSI nephelometer [10], is transformed into a two-step calibration process: First, minimizing the filtered air background and wall scattering (W). Second, adjusting the constant C, represented in the software as an empirical factor, to match the observed signal with the known scattering coefficient of CO_2 (relative to that of the filtered air) when this gas fills the IN. It should be emphasized that the values of the parameters C and W differ from one alignment process to another. Typical values of these constants are $C = 0.1$ and $W = 50$ Mm^{-1}. As can be inferred from table 1, the IN has a wall scattering about five times lower than that of the ISIN.

Equation (4) is used to calibrate the IN using calibration gases as explained below. The signal measured by the IN is proportional to the optical power scattered by the aerosol between the two limiting scattering angles θ_1 and θ_2, which are determined by the geometry of the nephelometer. If $\theta_1 = 0^\circ$ and $\theta_2 = \pi$, then the signal would be proportional to the particulate scattering coefficient B_{sp} given by [29]

$$B_{sp} = 2\pi \int_{\theta_1}^{\theta_2} \beta_p(\theta)\sin(\theta)\,\mathrm{d}\theta, \tag{5}$$

where $\beta_p(\theta)$ is the particulate volume scattering function, which can be related to scattering by a population of particles with number concentration N and size distribution $N(D)$ by

$$\beta_p(\theta) = \int_0^\infty \frac{|S(\theta, x, m)|^2}{2\pi x^2}\frac{\pi D^2}{4}\frac{\partial N}{\partial \log D}\,\mathrm{d}\log D, \tag{6}$$

where $|S(\theta, x, m)|^2$ is the scattering intensity function for a single particle of size parameter x $\left(=\frac{\pi D}{\lambda}\right)$ and complex refractive index m.

The calibration of the IN follows the general principle of producing a medium of known scattering coefficient, and adjusting the reading of the instrument to the desired value. To measure an ideal scattering coefficient, a scattering signal integrated from 0° to 180° is required. According to an analysis done by Horvath and Kaller [30], for a typical atmospheric aerosol (mass mean diameter of the accumulation mode of 0.6 μm, coarse mode of 3 μm of equal mass), the values of the truncated integral equation (5) (with $\theta_1 = 8^\circ$ and $\theta_2 = 168^\circ$) and the full integral equation (5) (with $\theta_1 = 0^\circ$ and $\theta_2 = \pi$) at a wavelength of 550 nm differ by 10.5%, whereas for a purely Rayleigh scattering aerosol or a gas the difference is only 2.3%. Therefore, besides the common two gases calibration method, it may be helpful to use an aerosol calibration method to reduce differences in the truncation error and to extend the calibration range. In order to determine C accurately, the following two independent calibration methods are usually used.

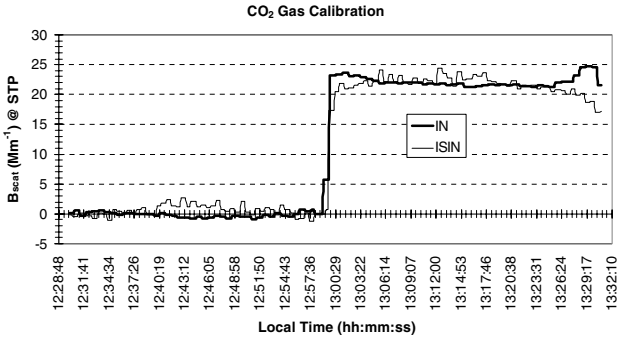

Figure 4. Time series of CO_2 scattering measurements for the IN and ISIN.

3.1. Gaseous calibration

In this commonly used method, two span gases with well-known but different scattering coefficients are utilized. The scattering coefficients of the two pure gases are plotted against their corresponding PMT output voltages to establish a linear response relationship. Due to the wall scattering, the line, in general, does not pass through the origin. Then, in principle, the scattering coefficient of any other medium can be extrapolated.

The IN has sufficient sensitivity, stability and linearity to discern between particle-free air and CO_2 gas on the basis of their Rayleigh scattering properties with a $\frac{S}{N} \approx 406$ at an electronic time constant of 10 s. The calibration procedure is simple. Particle-free air is first introduced into the system through a filter to provide the first calibration point and the reading is set to zero to subtract both air and wall scattering. Then particle-free CO_2 is passed through the same filter to register the value. Next, the calibration factor is adjusted and the procedure is repeated (if necessary) until the measured scattering coefficient of CO_2 matches the known calibration value, as the difference of scattering by CO_2 and air. Figure 4 shows the CO_2 IN-B_{scat} signal as compared with that of the ISIN and as referenced to filtered air as a function of time. Initially, air is drawn simultaneously into the nephelometers through a common filter. To eliminate the background wall scattering for each nephelometer, the PMT signal is measured with particle-free air and is subtracted from the subsequent scattering measurements. During the first 30 min, both nephelometers monitored particle-free air; thus the signals reflect the noise in the systems. As can be estimated

from the calibration graph of figure 4, during the first 30 min, signals of the IN and ISIN are about 0 ± 1 Mm^{-1} and 0 ± 3 Mm^{-1} for a time constant of 10 s, respectively. Then CO_2 gas is passed simultaneously to both nephelometers through the same filter. The IN took about 43 s to register the known CO_2 gas scattering coefficient while the ISIN took about 105 s before the sampling volume was filled and stable measurements could be made. Hence, the IN samples about 2.4 times faster than the ISIN does. This difference in time response is due to the IN smaller sampling volume. It should be mentioned that the IN and the ISIN sample at rates of about 3 l min^{-1} and 10 l min^{-1}, respectively. The IN flow rate could be further increased without reaching the turbulence threshold. In other words, the IN has a much shorter time response than the ISIN, thereby enhancing its real time capability. For both nephelometers, the CO_2 gas scattering signals are averaged over about 20 min. The measured CO_2 scattering coefficients, relative to particle-free air at STP, can be expressed using their mean values and standard deviations as 21.7 ± 0.0551 Mm^{-1} and 22.8 ± 0.132 Mm^{-1} for the IN and ISIN, respectively. The CO_2 gas scattering coefficient mean value of the IN agrees to within about 5% with that of the ISIN. The signal-to-noise ratio $\left(\frac{S}{N}\right)$ for both nephelometers is estimated using the formula

$$\frac{S}{N} = \frac{\langle V_{\mathrm{PMT}} \rangle}{\Delta V_{\mathrm{PMT}}} = \left[\left(\frac{\Delta B_{\mathrm{scat}}}{\langle B_{\mathrm{scat}} \rangle} \right)^2 - \left(\frac{\Delta P}{\langle P \rangle} \right)^2 \right]^{-\frac{1}{2}}. \qquad (7)$$

Here $\langle V_{\mathrm{PMT}} \rangle$, $\langle B_{\mathrm{scat}} \rangle$ and $\langle P \rangle$ represent the mean values of the PMT voltage, scattering coefficient and laser power, respectively, while ΔV_{PMT}, ΔB_{scat} and ΔP are their respective standard deviations. It is found that the $\frac{S}{N} \approx 406$ for the IN, and $\frac{S}{N} \approx 175$ for the ISIN.

3.2. White aerosols calibration

The scattering coefficients of particle-free air and CO_2 are generally lower than the aerosol coefficients in an urban area of average pollution. Thus another calibration method extending the calibration range is desirable.

The transmittance (T) of monochromatic light through the IN can be expressed by the Beer–Lambert law for optical depths much less than unity as

$$T = \frac{P}{P_0} = \exp(-B_{\mathrm{ext}}\ell) = \exp[-(B_{\mathrm{scat}} + B_{\mathrm{abs}})\ell], \qquad (8)$$

where P_0 is the power of the incident beam, P is the transmitted laser power and $\ell = 100$ cm is the extinction length (window-to-window distance) and B_{abs} and B_{ext} are the absorption and extinction coefficients, respectively. If the sampling volume of the IN is filled with white aerosol (no light absorption), then B_{scat} and B_{ext} are equal. Both ammonium sulfate $(NH_4)_2SO_4$ and sodium chloride (NaCl) salts can be considered as non-absorbing aerosols. Their refractive indices at $\lambda = 0.5$ μm are $m = (1.52\text{–}1.54, \sim 10^{-7})$ and $m = (1.55, \sim 10^{-7})$, respectively [31]. Given that $\ell = 100$ cm and P_0 and P can be measured, the left-hand equality of equation (8) can be used to determine B_{ext}. Monitoring B_{ext} can now be used to calibrate B_{scat} measured in the same sample volume with equation (8) becoming the basis for the scheme to extend and check the linearity of the IN gaseous calibration. While gaseous calibration methods are limited to a small range of scattering coefficients and need to assume a linear response beyond this range, the non-absorbing aerosol calibration method described here can utilize a much wider range and number of scattering coefficients by using various aerosol dilutions. Therefore, the non-absorbing aerosol calibration method complements the commonly used calibration method of utilizing air and CO_2 for calibration. Both nephelometers were calibrated using dry non-absorbing aerosols. $(NH_4)_2SO_4$ and NaCl salts were generated with an ultrasonic humidifier (UH) and subsequently dried. With the increase of the relative humidity (RH), the uptake of water causes an increase in both particle mass and size and a decrease in the refractive index; the net effect of all these factors is an increase in light scattering. To keep the RH-induced effects minimal, the RH of both calibration aerosols was kept within a range of 15–20%. In commercial nephelometers that utilize a thermal light source to illuminate the scattering volume [10], temperature gradients associated with heating caused by the light source produce significant RH-gradients within the sampling chamber. In our IN, this effect is significantly reduced by adopting the laser-based reciprocal design. Figure 5(*a*) shows an $(NH_4)_2SO_4$ time-series intercomparison between the IN-B_{scat}, IN-B_{ext} and the ISIN-B_{scat} with a 30 s time resolution. The calibration experiment started at 16:00 local time and finished at 17:30. During the 1.5 h run, three main scattering (extinction) ranges were encountered: 0–40 000 Mm^{-1}, 40 000–70 000 Mm^{-1} and 110 000–130 000 Mm^{-1}. Although the extinction measurements were noisy below about 10 000 Mm^{-1}, all values are included. In the time period 16:00–16:50, IN-B_{scat} and ISIN-B_{scat} agree very well while the IN-B_{ext} is

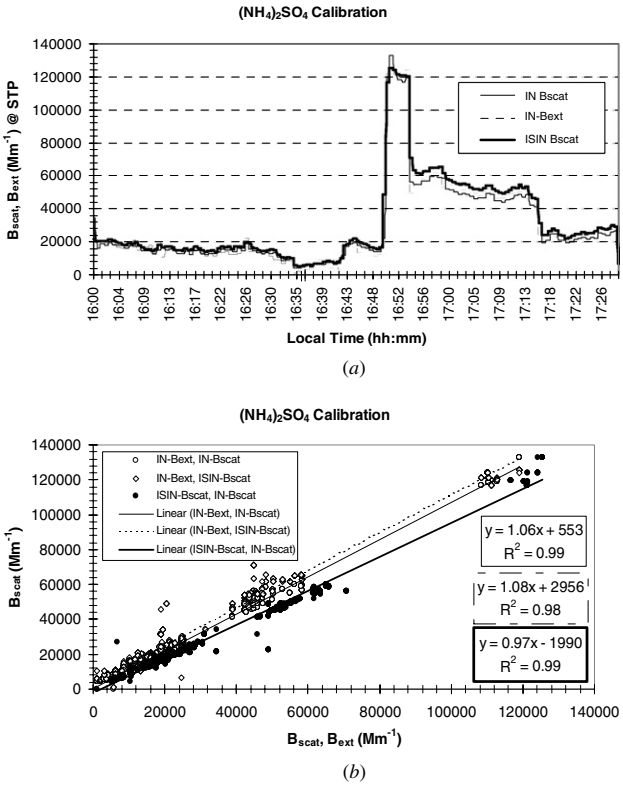

Figure 5. Ammonium sulfate calibration: (*a*) time-series comparison between IN-B_{scat}, IN-B_{ext} and ISIN-B_{scat}; (*b*) correlation between IN-B_{scat}, IN-B_{ext} and ISIN-B_{scat}.

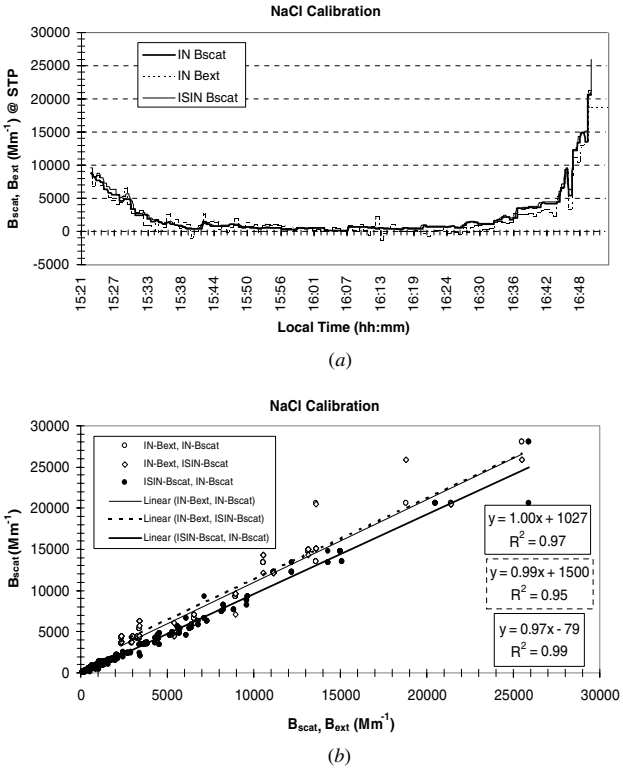

Figure 6. Sodium chloride calibration: (*a*) time-series comparison between IN-B_{scat}, IN-B_{ext} and ISIN-B_{scat}; (*b*) correlation between IN-B_{scat}, IN-B_{ext} and ISIN-B_{scat}.

noisy between 16:32 and 16:37. Figure 5(*b*) demonstrates quantitatively the relationship between (IN-B_{scat}, IN-B_{ext}), (ISIN-B_{scat}, IN-B_{ext}) and (IN-B_{scat}, ISIN-B_{scat}). Ideally, the trendlines of these graphs should have a slope of one, zero-offset and correlation coefficient (R^2) of 1. Figure 5(*b*) shows excellent correlation ($R^2 = 0.99$) between B_{scat} and B_{ext} monitored continuously over the same sampling volume of the IN and good quantitative agreement with a regression slope within 6% of one and an offset of less than 0.42% of the maximum value. Likewise, it shows a high correlation ($R^2 = 0.98$) between the ISIN-B_{scat} and IN-B_{ext}, good quantitative agreement with a regression slope within 8% of one and an offset of 2.26% of the maximum value. Also, it shows an excellent correlation ($R^2 = 0.99$) between IN-B_{scat} and ISIN-B_{scat}, excellent quantitative agreement with a regression slope within 3% of one and an offset of 1.50% of the maximum value. To increase confidence, the white aerosol calibration method is also evaluated with NaCl. Figure 6(*a*) plots a time-series intercomparison between the two nephelometers' coefficients over about 88 min. As can be seen from this plot, the extinction measurements are very noisy below a scattering coefficient of about 8220 Mm^{-1}, and thus were excluded throughout (15:23–16:40). During the same period, the scattering coefficients show a similar pattern. During the last 10 min of the run, the concentration of NaCl aerosol was enhanced to reduce the noise in the extinction measurements to check the calibration. Consequently, the IN-B_{ext} is increased from 2350 Mm^{-1} at 16:40 to 25 500 Mm^{-1} at 16:50. Figure 6(*b*) demonstrates, quantitatively, the relationship between (IN-B_{scat}, IN-B_{ext}), (ISIN-B_{scat}, IN-B_{ext}) and (IN-B_{scat}, ISIN-B_{scat}), respectively. It shows an excellent correlation ($R^2 = 0.97$) between B_{scat} and B_{ext} monitored continuously over the same sampling volume of the IN and an excellent quantitative agreement with a regression slope within 0% of one and an offset of less than 3.67% of the maximum value. Likewise, it shows a high correlation ($R^2 = 0.95$) between the ISIN-B_{scat} and IN-B_{ext}, very good quantitative agreement with a regression slope within 1% of one and an offset of 5.36% of the maximum value. Also, it shows an excellent correlation ($R^2 = 0.99$) between IN-B_{scat} and ISIN-B_{scat}, very good quantitative agreement with a regression slope within 4% of one and an offset of 0.28% of the maximum value. As can be inferred from table 2, in both cases of the $(NH_4)_2SO_4$ and the NaCl calibration runs, the scattering coefficients of the IN are lower than those of the ISIN by 3% and 4%, respectively.

4. Kerosene soot measurements

Soot particles are a product of the incomplete combustion of hydrocarbon fuels and consist mostly of elemental carbon (EC) and organic carbon (OC) often in the form of primary EC spherules of 20–50 nm diameter arranged in fractal-like chain aggregates and coated with OC. The optical properties of soot are determined by particle size, morphology and complex refractive index. OC scatters light without much absorption in the visible, while EC is a strong absorber across the spectrum. In the literature, a variety of values can be found for the complex refractive index of soot, most likely caused by different production methods and thus composition of the particles. At $\lambda = 0.55$ μm, the data range from (1.25, 0.25) to (2.67, 1.34) [32]. Following an analysis done by Chang and Charalampopoulos [33], at $\lambda = 532$ nm, the calculated refractive index of soot is (1.73, 0.60). In this case, $B_{ext} \neq B_{scat}$, thus only the scattering coefficients of the IN and ISIN can be compared.

Kerosene soot is generated in the laboratory in a controlled manner and is diluted as necessary. Figure 7(*a*) plots a time-series comparison between IN-B_{scat} and the ISIN-B_{scat}. During the period 11:00–14:30, many concentration levels are encountered providing scattering coefficients in the range of 10–2270 Mm^{-1}. As can be seen, during the 3 h run though both scattering coefficients are very variable they have excellent pattern match, throughout almost every scattering level. Figure 7(*b*) demonstrates an excellent correlation ($R^2 = 0.98$) and excellent quantitative agreement with a regression slope within 3% of one and an offset of less than 0.2% of the maximum value. Thus the slope of the soot (IN-B_{scat}, ISIN-B_{scat}) run shows a perfect (0% difference) agreement with that of the $(NH_4)_2SO_4$ run. In addition, it shows an excellent (1% difference between slopes) agreement with that of the NaCl calibration run.

5. Ambient measurements and comparison with the integrating sphere integrating nephelometer

For comparison, the IN was set up near to the ISIN during the measurements. Both nephelometers were operated using two similar computer programs whose outputs are compared by a

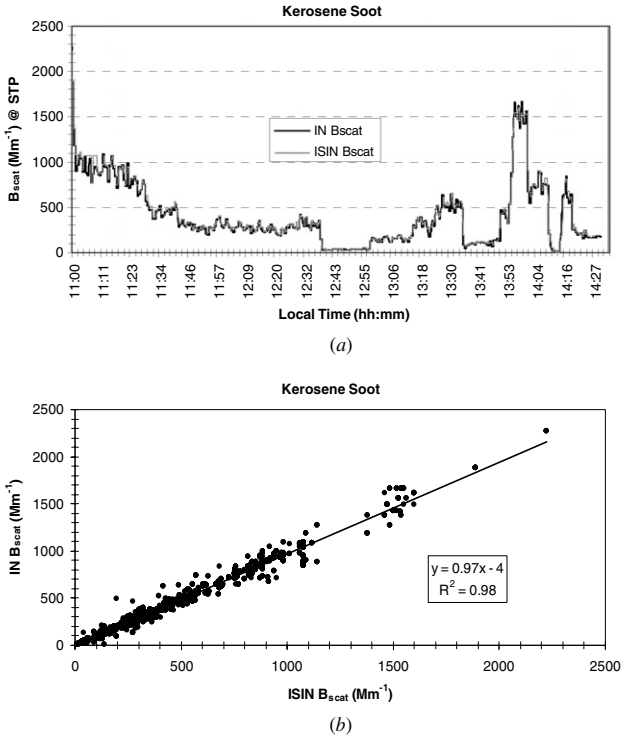

Figure 7. Kerosene soot measurements: (*a*) time-series comparison between IN-B_{scat} and ISIN-B_{scat}; (*b*) correlation between IN-B_{scat} and ISIN-B_{scat}.

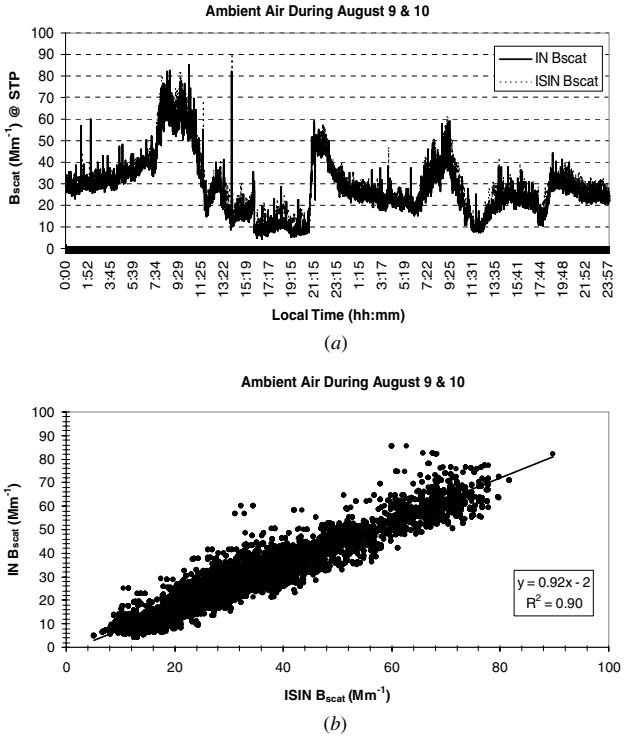

Figure 8. Ambient air measurements: (*a*) time-series comparison between IN-B_{scat} and ISIN-B_{scat}; (*b*) correlation between IN-B_{scat} and ISIN-B_{scat}.

third one. The data were averaged for the same periods (30 s). This experiment was performed on 9 and 10 August 2004 in the Optics and Acoustic Laboratory of the DRI, Reno, NV. The ambient aerosol intake was a 1.91 cm outer diameter copper tube inserted through the laboratory wall at ∼10 m above the ground. Parking lots are nearby, and a busy highway is within 1 km of the inlet. During the two-day run, sufficiently different scattering levels and atmospheric conditions were encountered to give an initial indication of the accuracy limits of the aerosol scattering measurements in the IN. All measurements were converted to standard temperature and pressure conditions and the filtered air background is periodically and automatically checked and adjusted. Figure 8(*a*) shows the light scattering coefficients for both nephelometers versus time of day. The scattering coefficient measurements both by IN and the ISIN show a similar trend. During the 48 h run, scattering coefficients ranging from about 5 Mm^{-1} to about 85 Mm^{-1} are measured. This scattering range is within the noise level of the extinction measurements (±8220 Mm^{-1}); therefore, no comparisons with the IN-B_{ext} were performed. In particular, one interesting and illustrative feature in figure 8(*a*) is that the two curves match almost the same way for both high and low scattering coefficient limits. However, figure 8(*b*) reveals that the IN-B_{scat} is lower by about 8% than that of the ISIN. The IN-B_{scat} correlates well ($R^2 = 0.90$) with the ISIN-B_{scat}. The offset is about 1.87% of the maximum value. As can be inferred from table 2, (IN-B_{scat}, ISIN-B_{scat}) comparison for ambient aerosol shows a slope that is about 5%, 4%, 5% lower than those of kerosene soot, NaCl and $(NH_4)_2SO_4$, respectively. This discrepancy between the slopes of the ambient run and those of calibration runs is within the uncertainty limit (±8%) of the white aerosol calibration runs.

6. Conclusions

A prototype of a low truncation angle reciprocal IN has been described. In addition, a simple experimental setup for the measurement of a reciprocal IN sensor's angular response and truncation angle has been developed. This setup is demonstrated by characterizing the response of a commercially available physical cosine corrector. The collection geometry of the original cosine corrector is improved, reducing its truncation angle to 4°. This modified physical cosine corrector is employed as a sensor in the IN. The performance of the IN is evaluated, at a wavelength of 532 nm, through extensive comparison with a 1° truncation angle reciprocal ISIN that operates at the same wavelength. The intercomparison included measurements of ambient aerosol, kerosene soot, ammonium sulfate aerosol, NaCl aerosol and CO_2 gas. Results of linear regression analysis indicate discrepancies within a range of ±8% between the IN and the ISIN. The IN has a S/N of 406, which is substantially larger than that of the ISIN (i.e. 175). In addition, a white aerosol extinction-scattering calibration method has been demonstrated for the IN, greatly extending the calibration range.

Acknowledgment

This work was funded in part by the National Science Foundation, grant ATM-0216572.

References

[1] Vedal S 1997 Critical review—ambient particles and health: lines that divide *J. Air Waste Manage. Assoc.* **47** 551–81

[2] Watson J G 2002 Visibility: science and regulation *J. Air Waste Manage. Assoc.* **52** 626–713

[3] Jacob D J 1999 *Introduction to Atmospheric Chemistry* (Princeton, NJ: Princeton University Press) p 146

[4] Beuttell R G and Brewer A W 1949 Instruments for the measurement of the visual range *J. Sci. Instrum.* **26** 357–9

[5] Ahlquist N C and Charlson R J 1967 A new instrument for evaluating the visual quality of air *J. Air Pollut. Control Assoc.* **17** 467–9

[6] Charlson R J 1980 The integrating nephelometer *Atmos. Technol.* **12** 10–4

[7] Gerber H E 1979 Portable cell for simultaneously measuring the coefficients of light scattering and extinction for ambient aerosols *Appl. Opt.* **18** 1009–14

[8] Mulholland G W and Bryner N P 1994 Radiometric model of the transmission cell-reciprocal nephelometer *Atmos. Environ.* **28** 873–87

[9] Peñaloza M A 1999 Deriving the basic cell-reciprocal integrating nephelometer equation and its use for calibration purposes: a comprehensive approach *Meas. Sci. Technol.* **10** R1–5

[10] Anderson T L *et al* 1996 Performance characteristics of a high-sensitivity, three-wavelength, total scatter/backscatter nephelometer *J. Atmos. Ocean. Technol.* **13** 967–86

[11] Quenzel H 1969 Der Einfluss der Aerosolgrößenverteilung auf die Messgenauigkeit von Streulichtschreibern. *Gerlands Beitr. Geophys.* **78** 251–63

[12] Ensor D S and Waggoner A P 1970 Angular truncation error in the integrating nephelometer *Atmos. Environ.* **4** 481–7

[13] Heintzenberg J and Quenzel H 1973 On the effect of the loss of large particles on the determination of scattering coefficients with integrating nephelometers *Atmos. Environ.* **7** 503–7

[14] Rabinoff R A and Herman B M 1973 Effect of aerosol size distribution on the accuracy of the integrating nephelometer *J. Appl. Meteorol.* **12** 184–6

[15] Quenzel H, Ruppersberg G H and Schellhase R 1975 Calculations about the systematic error of visibility meters, measuring scattered light *Atmos. Environ.* **9** 587–601

[16] Harrison A W 1979 Nephelometer estimates of visual range *Atmos. Environ.* **13** 645–52

[17] Sokolik I and Golitsyn G 1993 Investigation of optical and radiative properties of atmospheric dust aerosols *Atmos. Environ.* **27A** 2509–17

[18] Chakrabarty R *et al* 2006 Emissions from the laboratory combustion of wildland fuels: particle morphology and size *J. Geophys. Res.* **111** 7204–20

[19] Draine B T and Flatau P J 1994 Discrete-dipole approximation for scattering calculations *J. Opt. Soc. Am.* A **11** 1491–9

[20] Xu Y 1998 Electromagnetic scattering by an aggregate of spheres: asymmetry parameter *Phys. Lett.* A **249** 30–6

[21] Xu Y 2003 Radiative scattering properties of an ensemble of variously shaped small particles *Phys. Rev.* E **67** 046620

[22] Moosmüller H and Arnott W P 2003 Angular truncation errors in integrating nephelometry *Rev. Sci. Instrum.* **74** 3492–501

[23] Anderson T L and Ogren J A 1998 Determining aerosol radiative properties using the TSI 3563 integrating nephelometer *Aerosol Sci. Technol.* **29** 57–69

[24] Varma R, Moosmüller H and Arnott W P 2003 Toward an ideal integrating nephelometer *Opt. Lett.* **28** 1007–9

[25] Strawa A *et al* 2003 The measurement of aerosol optical properties using continuous wave cavity ring-down techniques *J. Atmos. Ocean. Technol.* **20** 454–65

[26] Arnott W P 2004 personal communication

[27] Moosmuller H *et al* 2005 Scattering cross-section emissions: military vehicles traveling on unpaved roads *J. Air Waste Manage. Assoc.* **55** 1743–50

[28] Sheridan P J *et al* 2005 The Reno aerosol optics study: an evaluation of aerosol absorption measurement methods *Aerosol Sci. Technol.* **39** 1–16

[29] Middleton W E K 1952 *Vision Through the Atmosphere* (Toronto: University of Toronto Press) p 250

[30] Horvath H and Kaller W 1994 Calibration of integrating nephelometers in the post-halocarbon era *Atmos. Environ.* **28** 1219–23

[31] Toon O B, Pollack J B and Khare B N 1976 The optical constants of several atmospheric aerosol species: ammonium sulfate, aluminum oxide and sodium chloride *J. Geophys. Res.* **81** 5733–48

[32] Fuller K A, Malm W C and Kreidenweis S M 1999 Effects of mixing on extinction by carbonaceous particles *J. Geophys. Res.* **104** 15941–54

[33] Chang H and Charalampopoulos T T 1990 Determination of the wavelength dependence of refractive indices of flame soot *Proc. Math. Phys. Sci.* **430** 577–91